Journal of Applied Mechanics and Technical Physics, Vol. 45, No. 3, pp. 428–439, 2004

STABILITY, PATHS, AND DYNAMIC BENDING OF A BLUNT BODY OF REVOLUTION PENETRATING INTO AN ELASTOPLASTIC MEDIUM

I. V. Simonov and K. Yu. Osipenko

UDC 539:374:629.7

The deep penetration of a thin body with a blunt nose and rear into a low-strength medium is explored. The motion of the body is described by a system of autonomous integrodifferential equations using the physical model of a separated asymmetric flow over the body and the local-interaction method. An analytical calculation of the Lyapunov stability boundary for straight-line motion is performed for bodies with a parabolic meridian. The dependences of the dynamic stability of the body on various parameters are studied numerically. Curved motion paths are constructed in the region of instability, and the classification of paths proposed in previous studies of the motion of pointed bodies is confirmed. It is shown that an reverse ejection is possible when a blunt impactor enters a semi-infinite target. It is established that there is a fundamental possibility of attaining a path close to a specified one and that there is a weak dependence of motion characteristics with a developed separation on the separation angle. Examples are given of calculations of the evolution of the lateral load, the transverse force and moment, and the strength margin of the body using the theory of dynamic bending of a nonuniform rod.

Key words: *penetration, impactor, elastoplastic medium, motion paths, flow separation, stability.*

Introduction. Direct penetration of a body of revolution has been studied analytically taking into account cavitation [1–3], and non-one-dimensional motion has been investigated numerically [4]. The deep penetration phenomenon has been used as the basis in developing various technologies, such as research stations for studying space objects [5, 6], controlled action on volcanic and seismic activities [7], etc. In this connection, penetration calculations, body shape optimization, and stability analysis of body motion have gained fundamental importance.

In hydrodynamics, flow separation and motion stability are among fundamental problems. The complex nature of interaction forces and the cavitation nature of flows even at low velocities hinder investigation of the non-one-dimensional motion of bodies in high-strength media and make it impossible to solve these problems in exact formulations [1]. Numerical methods for solving problems in exact formulations are effective in studies of the initial stage of impact and penetration, but, because of a large number of parameters and determining functions, the results are of a simulation nature and are unsuitable for finding general regularities. In addition, because of low measurement accuracy and the instability of dynamic properties of materials, in particular, geological media, the requirements for modeling accuracy can be reduced. Therefore, it is justified to use approximate approaches based on a phenomenological description of the interaction of a medium and a body with a corresponding "calibration" of the model.

In the present study, we consider the physical model of a separated flow over a body based on an analysis of local interaction [8] (the isolated element method in mathematics). Explicit specification of coefficients as functions of parameters of the medium using asymptotically exact solutions [9, 10] and results of experiments [11, 12] made it possible to estimate the coefficients, to perform an asymptotic analysis, and to simplify the system of autonomous integrodifferential equations of body motion (resolved for derivatives) for which the Cauchy problem is formulated.

Institute of Problems of Mechanics, Russian Academy of Sciences, Moscow 119526. Translated from Prikladnaya Mekhanika i Tekhnicheskaya Fizika, Vol. 45, No. 3, pp. 146–160, May–June, 2004. Original article submitted August 18, 2002; revision submitted March 13, 2003.

For bodies of a parabolic shape, an analytical calculation of the Lyapunov stability boundary of straight-line motion is performed (this problem was generally solved in [13]). Numerical studies are made of the dependences of body motion stability on initial deviations from the normal entry conditions, the "frozen" axial velocity, body shape, separation angle (a parameter included in the empirical separation criterion), and the position of the center of mass of the body in comparison with the stability criteria in the small. Curved motion paths are constructed in the region of instability taking into account deceleration, and the classification of the paths proposed in studies [14] of the motion of pointed bodies is confirmed. It is shown that the entry of a blunt impactor into a semi-infinite target can lead to an reverse ejection, as was previously detected in the unpublished experiments of Yu. K. Bivin.

The separation hypothesis is based on observations of body motion in low-strength media: ideal separation occurs in the midlength section at low velocities; an empirical separation angle is introduced for high velocities and in the presence of initial stresses. The examined range of velocities is determined by the same order of magnitude of contributions from hydrodynamic and strength resistances. In this case, there is a deep (far exceeding the body length) penetration of a high-strength massive thin impactor.

1. Physical Description and Hypotheses. An oblong blunt body of revolution moves inertially in an unbounded isotropic and homogeneous elastoplastic medium. The length scale in the longitudinal and transverse directions are the body length L and its maximum radius $r_{\max}$, respectively. The dimensionless equation of the meridian is written in the cylindrical coordinate system (R, φ, l): $R = R(l) = r/r_{\max}$, which is rigidly attached to the body and the local rectangular coordinates $x = l_c - l$, $y = R\cos\varphi$, and $z = R\sin\varphi$ (l is the distance from the body nose; $R_0 \leqslant R \leqslant 1$; $0 \leqslant l \leqslant 1$; R_0 is the bluntness radius; and $l = l_c$ and $R = 0$ are the coordinates of the center of mass). The thin-body conditions

$$\varepsilon = r_{\max}/L \ll 1, \qquad \varepsilon\beta \ll 1, \qquad \beta = R' = dR/dl, \qquad l_n < l < 1 \tag{1}$$

are satisfied everywhere except in a small neighborhood of the nose $0 \leqslant l \leqslant l_n \ll 1$, which is neglected in the calculations.

At the initial time $t = 0$, the velocity $\boldsymbol{v}_0$ of the center of mass of the body and the angular velocity of rotation Ω_0 about this center are specified. We assume that rotation begins in the plane formed by the velocity $\boldsymbol{v}_0$ and the body axis (yaw and other rotations are absent). Then, the paths of points of the body are two-dimensional if the dynamic properties of the body possess rotational symmetry.

Let us designate the current translation, angular, and complete velocities and the current velocity normal to the body surface by $\boldsymbol{v} = (v_x, v_y, 0)$, $\boldsymbol{\Omega} = (0, 0, \Omega)$, $\boldsymbol{V} = \boldsymbol{v} + \boldsymbol{\Omega} \times (x, y, z)$, and $V_n = \boldsymbol{n}\boldsymbol{V} = \varepsilon\,\delta v_x$, respectively ($\boldsymbol{n}$ is a unit normal to the surface):

$$\delta = \beta - a\cos\varphi, \qquad a = -\omega x - \eta, \qquad \omega = \Omega L/(\varepsilon v_x), \qquad \eta = v_y/(\varepsilon v_x). \tag{2}$$

The dimensionless angular velocity ω and the angle of attack η are normalized so that in the asymptotically exact model being constructed, they can take values $O(1)$ with error $O(\varepsilon^2)$. The mass of the body m is expressed in terms of the dimensionless length of a cylinder with equivalent mass and midlength section l_e and the mean density of the body ρ_1: $m = \pi r_{\max}^2 L l_e \rho_1$. The incompressible medium is characterized by the density ρ_0, the shear modulus μ, and the Mises dynamic yield point τ_d. For plastically compressed (porous) media, it can be assumed that the medium becomes continuous at a considerable distance from the body with density ρ_0 in this state.

According to the results of [9, 10], a plastic zone with a "large" characteristic dimension $\sqrt{\mu/\tau_d}\ R(l)$ is formed near the contour. Intense shear flow and flow separation occur near the contour. At low velocities, viscous near-wall effects are observed. At moderate velocities (over 1 m/sec for wet clay soil) and high velocities, the material slides along the impactor walls and agreement between theoretical and experimental results is achieved by choosing a plastic friction law [11, 12]. According to the model of [13], separation arises when the slope of the body surface element to the flow velocity vector at infinity reaches the critical value [12]

$$\delta^* \equiv \delta - \beta_*(\sigma_{ij}^0, V) = 0. \tag{3}$$

At subsonic velocities, while the inertial motion of the medium is insignificant, the separation is ideal and occurs in the midlength section near the rear boundary of the body ($\beta_* = 0$). With increase in the velocity, the separation angle increases, and with increase in the initial compressing stresses σ_{ij}^0 in the medium, it decreases. A simple procedure for determining β_* in the experiment was proposed in [15].

We shall distinguish the wetting S_+ ($\delta^* > 0$) and the separation zone S_- ($\delta^* < 0$), in which the stresses are equal to zero; $S = S_+ + S_-$ is the total surface area of the body (Fig. 1). We shall restrict ourselves to regimes

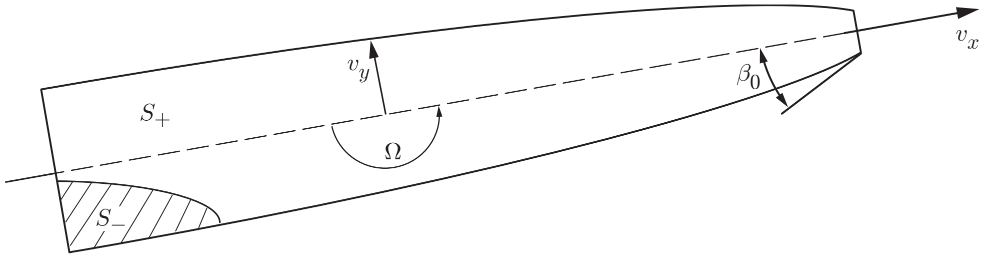

Fig. 1. Elastoplastic flow over a blunt body.

without jet attachment. The influence of initial stresses and associated mass on the resultant forces is neglected [11, 12].

We partition the surface S into elements and approximate them by the surface of one of the canonical forms (a sphere, a cone, or a cylinder). The contact stress vector $\boldsymbol{\Sigma}$ on the wetted element of the body surface is defined, according to the local interaction model [8] (supported theoretically in [9] and experimentally in [11, 12]) by the sum of contributions of the hydrodynamic and strength terms:

$$S_+:\quad \boldsymbol{\Sigma} = \tau_S \boldsymbol{n}_\tau - \sigma_n \boldsymbol{n}, \quad \sigma_n = C_x \rho_0 V^2/2 + b\tau_d, \qquad S_-:\quad \Sigma = 0.$$

Here $\tau_S = \text{const} \leqslant \tau_d$ is the plastic friction law; $\boldsymbol{n}_\tau$ is a unit vector in the sliding direction (in the approximation considered, $\boldsymbol{n}_\tau = (-1, 0, 0)$; and $\sigma_n > 0$ is the contact pressure. The coefficients C_x and b can be varied and specified from experiments or from solutions of model flow problems. Thus, on the flat segments of the lateral surface S_f, where $\delta \ll 1$, we assume [9]

$$C_x(S_f) = C_f \delta^2 \varepsilon^2, \qquad C_f = \ln(\mu/\tau_d) + 2.55, \qquad b = b_f = \ln(4\mu/\tau_d) - 1.$$

The quadratic law is valid to values $C_x \leqslant 0.2$, and the formulas for C_f and b_f were obtained by solving the problem of a thin cone subject to the condition of $\varepsilon\delta \ll (\tau_d/\mu)^{1/2}$ ($\varepsilon\delta < 10^{-2}$). In the region $\varepsilon\delta \sim 10^{-1}$ we can assume the value $C_f = 2.9$, fitted to the experiments of [12]. As a consequence of the approximate nature of the model, physical condition of separation $\sigma_n = 0$ is violated since σ_n in this case is the average value on the surface element.

For $0 \leqslant l \leqslant l_n$ and small perturbations, the frontal surface $S_\perp$ is entirely wetted and on this surface as on a unified element, $C_x = C_\perp$ and $b = b_\perp$. For cones with opening semiangles 15–90°, the coefficient $C_x = 0.18$–0.82 (subsonic velocities) is close to its hydrodynamic value [12] and the value of b depends weakly on the shape (changes by only 8%) and is approximately 2/3 of the value of b calculated by the formula for the maximum normal stress at the stagnation point of an elastoplastic flow over a sphere [10] (the exact formula for the case of a sphere and a cylinder is given in [15]). The typical values are $\mu/\tau_d = 10^2$–10^3; therefore, $b_f = 5$–8, $b_\perp = 16$–24 for $\delta > 0.1$. For the case of supersonic penetration into a porous medium, the pressure on the cone was found in [16].

The yield point τ_d as a parameter of the process is a factor of 1.5–2 higher than its static value [11, 12] and ceases to depend on the loading rate at velocities over 1 m/sec for a number of geological media. The reasons for the difference between τ_d and τ_S can be heating of the medium near the contour due to friction or forced heating of the body up to melting (vaporization).

In the model, only one parameter — the separation angle β_* is not determined; its influence will be studied parametrically. In addition, since a number of assumptions are insufficiently justified, the values of C_f, b_f, τ_d, and τ_S should be refined in control experiments.

2. Mathematical Formulation of the Problem. We introduce the following dimensionless variables and parameters:

$$æ = \frac{c^2}{v_x^2}, \qquad \xi = \int \frac{v_x\,dt}{L}, \qquad c^2 = \frac{2b_f\tau_d}{\varepsilon^2\rho_0 C_f},$$
$$D = \frac{\rho C_f}{2\pi l_e}, \quad \rho = \frac{\rho_0}{\rho_1}, \quad j_0 = \frac{mL^2}{J}, \quad \tau = \frac{\tau_S}{\varepsilon b_f \tau_d}, \quad A_1 = \pi R_0^2 \frac{DC_\perp}{\varepsilon^2 C_f}, \quad A_2 = \pi D R_0^2 \frac{b_\perp}{b_f} \tag{4}$$

(J is the principal moment of inertia of the transverse rotation).

For the functions æ, η, and ω defined by (2) and (4), the equations of motion of the body reduce to an autonomous system of integrodifferential equations resolved for ordinary derivatives, for which the Cauchy problem is formulated:

$$
\begin{gathered}
æ' = 2æ\varepsilon^2(A_1 + A_2æ + f_æ - \omega\eta), \qquad \eta' = f_\eta - \omega, \qquad \omega' = j_0 f_\omega, \\
\boldsymbol{æ} = (æ, \eta, \omega) = \boldsymbol{æ}_0, \qquad \xi = 0;
\end{gathered} \tag{5}
$$

$$
\begin{gathered}
\boldsymbol{f} = (f_æ, f_\eta, f_\omega) = D \int\limits_{S_+} (\tau æ + \beta\sigma, -\sigma\cos\varphi, -\sigma x\cos\varphi) R\, dl\, d\varphi, \\
f_æ = D \int\limits_0^1 \Theta R\, dl, \qquad (f, f_\omega) = D \int\limits_0^1 (1, l_c - l)\Phi R\, dl, \\
\Theta = \varphi_0\Theta_1 + \Theta_2, \qquad \Phi = 2a\beta\varphi_0 + \Psi\,\mathrm{sgn}\, a, \qquad 0 < l < 1, \\
\Theta_1 = 2(æ\tau + æ\beta + \beta^3) + \beta a^2, \qquad \Theta_2 = \beta|a|(4\beta - \beta^*)\sqrt{1 - q^2} H(1 - q)^2, \\
\Psi = [2æ + \beta^2 + a^2(2 + q^2)/3 - \beta\beta^*]\sqrt{1 - q^2}\, H(1 - q)^2, \qquad q = \beta^*/a, \\
\varphi_0 = \begin{cases} \pi, & q\,\mathrm{sgn}\, a \geqslant 1, \\ 0, & q\,\mathrm{sgn}\, a \leqslant -1, \end{cases} \qquad \varphi_0 = \begin{cases} \pi - \varphi^*, & a > 0,\ |q| < 1, \\ \varphi^*, & a < 0,\ |q| < 1, \end{cases} \\
\sigma = æ + \delta^2, \qquad \beta^* = \beta - \beta_*, \qquad \varphi^* = \arccos q.
\end{gathered} \tag{6}
$$

Here H is a stepped function and the prime denotes differentiation with respect to ξ. In the expressions for the resultant force (6) with the terms $O(\varepsilon^2)$ dropped, it is possible to perform integration over the angle φ subject to condition (1), so that only ordinary integrals are retained. Nevertheless, the right sides of Eqs. (5) are nonlinear.

The solutions of Eq. (3) $\varphi^* = \arccos(\beta^*/a)$ define the boundaries of separation zones that are symmetric about the meridians $\varphi = 0$ and π and have extrema on these meridians. The formulas for the generalized distributed loads Θ and Φ describe all cases of flow of an arbitrary parallel: flow without separation ($\varphi_0 = \pi$) and complete ($\varphi_0 = 0$) or partial ($\varphi_0 \neq 0, \pi$) separation.

The unknowns functions $æ$, η, and ω depend on body shape and eight dimensionless parameters. The quantity $æ$ can be defined as the ratio of strength resistance to velocity head. During body motion, this ratio varies in the range $æ_0 < æ < \infty$; in this case, the solution of problem (5) asymptotically describes almost all stages of the decelerated motion of the body. For $æ \ll 1$, inertia predominates. These values of $æ$ correspond to the range of considerable supersonic velocities, in which the interaction model (6) becomes unsuitable and the penetration is accompanied by fracture of the thin body itself. For $æ \gg 1$, it is possible to ignore the influence of inertia in calculation of the resultants. Therefore, we assume $æ_0 = O(1)$. The order of magnitude of $æ$ is determined not only by the velocity but also by the strength of the medium. In this case, the value $æ_0 = O(1)$ can be obtained for low velocities, too. For a soil of moderate dynamic strength ($\tau_d = 5 \cdot 10^6$ Pa), the value $æ \approx 1$ corresponds to a velocity of a conical (15°) impactor $V \approx 700$ m/sec.

The Cauchy problem (5) and (6) was solved numerically using the Runge–Kutta method. The integrals were calculated by the trapezoid method taking into account the complex analytical behavior of the integrands (discontinuities, boundary-layer type regions). We restrict ourselves to specifying a body meridian in the form of the parabola segment

$$
\begin{gathered}
R(l) = R_0 + (1 - R_0)[\beta_0 l - (\beta_0 - 1)l^2], \\
\beta(l) = (1 - R_0)[\beta_0 - 2(\beta_0 - 1)l], \qquad 0 < l < 1.
\end{gathered} \tag{7}
$$

The body has a disk bluntness of radius R_0 with apex angle $\beta_0(1 - R_0)$. We fix the values $\varepsilon = 0.065$ and $C_\perp = 0.82$ and vary the parameters $æ_0$, β_0, β_*, D, τ, j, and l_c.

The stability of the straight-line motion of the body was examined by calculations for the "frozen" axial velocity $æ = \text{const}$. Mathematically, "freezing" is justified by the different asymptotic order of the right sides of Eqs. (5): $O(\varepsilon^2)$ in the equation for $æ$ and $O(1)$ in the remaining equations, which implies that for thin bodies, the lateral resistance exceeds the axial one. In practice, such motion is possible under application of an external compensating following force.

The body was assumed to enter the half-space without a splash, which influences the position of the bifurcation points of the solution for finite perturbations.

3. Dimensions of the Separation Zone and the Separation Criterion in the Small. We consider bodies with a separation localized near the rear point $l = 1$ for $\beta_* = \beta_1 = \beta(1)$. For the body shape (7), the maximum length of the Δ separation zone on the meridians $\varphi = 0$ (+ sign) or $\varphi = \pi$ (− sign) is determined from Eq. (3) subject to the condition of $0 \leqslant \Delta \leqslant 1$:

$$\Delta = \frac{(b_0 - 2)(1 - R_0) + \beta_* \pm (1 - l_c)\omega \mp \eta}{2(b_0 - 1)(1 - R_0) \pm \omega}, \qquad |\omega| < 2.$$

If both roots are outside the indicated interval, by analysis of the inequality $\delta^* < 0$ for the presence of a separation zone, we find $\Delta = 0$ or 1. For $\beta_* \leqslant \beta_1$ and small perturbations, the separation zone is localized near the separation boundary for symmetric flow $l = l_*$: $\beta(l_*) = \beta_*$.

The critical value of the position of the center of mass l_s is found by stability analysis in the small [1] taking into account the small asymmetric separation zones near a certain parallel $l = l_*$:

$$l_s = \frac{A_0 A_2 - A_1^2 + \zeta A_1}{\zeta A_0}, \qquad A_m = p_m + l_{*,m}\psi, \qquad \zeta = \frac{2l_e(R_0)}{\rho C_f} = \frac{1}{\pi D},$$

$$D = D_0\,\frac{l_e(0)}{l_e(R_0)}, \qquad \psi = \frac{æ + \beta_*^2}{e_0|\beta'(l_*)|}\,R(l_*), \qquad e_0 = \begin{cases} 2, & \beta_* = \beta_1,\ l_* = 1, \\ 1, & \beta_* < \beta_1,\ l_* < 1, \end{cases}$$

$$p_m = 2\int_0^{l_*} l_m R(l)\,dR(l), \qquad m = 0, 1, 2, \tag{8}$$

$$l_e = \int_0^1 R^2(l)\,dl = R_0^2 + 2R_0(1 - R_0)\Big(\frac{b_0}{2} - \frac{b_2}{3}\Big) + (1 - R_0)^2\Big(\frac{b_0^2}{3} - \frac{b_0 b_2}{2} + \frac{b_2^2}{5}\Big).$$

For $\varepsilon_0 = 1 - R_0 \to 0$, the asymptotics $l_s \to 1 + \varepsilon_0/\zeta(1) + O(\varepsilon_0^2)$ is valid: the values $l_s > 1$ are on the left in the neighborhood of the point $R_0 = 1$. This agrees with the statement that a cylinder and, generally, bodies that are asymptotically close to a cylinder exhibit absolute stability near the rear point $[\beta'(1) = \beta''(1) = 0]$ [13, 15]. The degradation of the Lyapunov method is explained by the fact that the formation of small separation zones near the rear points of such a body for $R_0 \to 1$ requires extremely small perturbations of η and ω, and for $R_0 = 1$, arbitrarily small perturbations lead to the appearance of asymmetric separation spots of finite area.

Calculations using formula (8) showed that the curves $l_s = l_s(R_0)$ are nonmonotonic: for $R_0 > 0.85$ there is a maximum, after which the curves approach the asymptotics indicated above (Fig. 2). It should be noted that the values $D_0 = 0.11$, 0.26, and 0.44 correspond to the penetration of impactors from a tungsten alloy, steel, and titanium into a clay medium ($\rho_0 = 1.65$ g/cm^3). The calculations show that the larger D_0 (the lighter the body), the higher the stability margin (Fig. 2).

It can be proved that for bodies with an increasing dependence $R(l)$, the stability margin increases with increase in the relative density ρ for both continuous and separated flows.

4. Stability in the Large. As in the case of pointed bodies [14], a numerical experiment shows that the solution bifurcates on a certain surface

$$l_i = l_i(æ_0,\ b_0, \ldots), \qquad l_a(æ,\ b_0, \ldots) \leqslant l_i \leqslant l_s(æ, b_0, \ldots)$$

in the phase space of parameters: the perturbations damp for $l_c < l_i$ and grow for $l_c > l_i$ (exponentially if the perturbations are small). For $l_c < l_a$ (l_a is the absolute critical value), the perturbations damp, and for $l_c > l_s$, they grow under any initial conditions. As perturbations decrease, the value of l_i tends from below to the limit l_s, according to the stability criterion in the small (8). For variation in R_0 on the segment 0–0.7 with a step 0.1 and fixed values $D_0 = 0.115$, $b_0 = 2$, $\beta_* = 0$, and $j = 5.5$, we have $l_i = 0.61256$, 0.59913, 0.58789, 0.578 02, 0.56789, 0.55513, 0.53742, and 0.52693, respectively.

Because of the weak convergence of the solution to the limit in the neighborhood of the bifurcation points, we needed to check the calculation accuracy and to perform the calculations up to the value $\xi \approx 2000$ to determine these points by the successive-approximation method. For $R_0 \geqslant 0.7$, it was not possible to find the value of l_a because of the weak damping (growth) of the solution as $\xi \to \infty$ in the neighborhood of the required point. Below we give some intermediate critical values of l_i for a pointed body under various initial conditions:

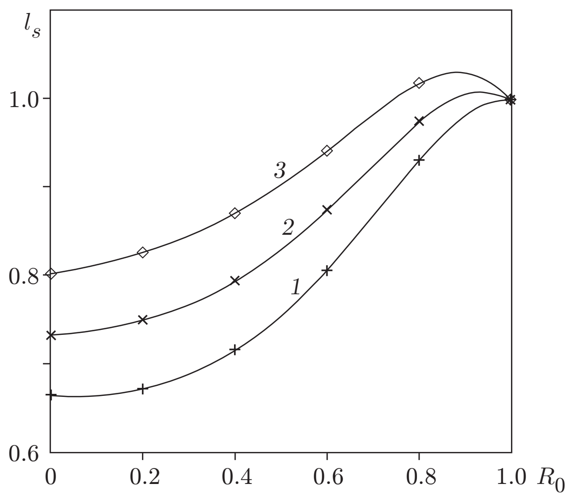

Fig. 2. Critical positions of the center of mass versus bluntness radius for æ = 2 and $D_0 = 0.01$ (1), 0.2 (2), and 0.5 (3).

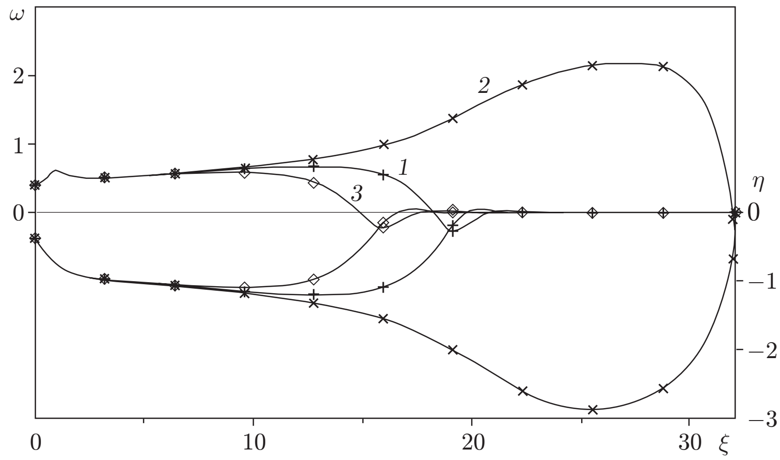

Fig. 3. Effect of computational instability of the solution near the bifurcation point $l_c = l_i$ ($l_c = 0.58795$, $æ_0 = 1$, $\omega_0 = -\eta_0 = 0.4$, $R_0 = 0.4$, $D_0 = 0.115$, and $\tau = 1.1$): $N_l = 400$ (1), 800 (2), and 1600 (3).

$$l_i = 0.61256 \quad \text{at} \quad \gamma_0 = (-0.5; 0.5), \qquad l_i = 0.66955 \quad \text{at} \quad \gamma_0 = (-0.1; 0.1),$$

$$l_i = 0.69335 \quad \text{at} \quad \gamma_0 = (-0.01; 0.01) \qquad [\gamma_0 = (\eta_0, \omega_0)].$$

The bifurcation interval of the solution $l_s - l_a$ increases in the presence of a bluntness, for example: $l_s - l_a \approx 0.092$ for $R_0 = 0$ and $l_s - l_a \approx 0.235$ for $R_0 = 0.5$. If the point l_c is located even at a small distance on the right of the critical point l_i, stabilization occurs rather rapidly: $\gamma, \Delta \to \gamma_*, \Delta_*$. The limiting cycle is always constant motion on a circle of asymptotically large radius $R_* = 1/(\varepsilon^2 \omega_*)$ as in the case of pointed bodies. As l_c increases, the amplitudes γ_* grow and the separation zone is immediately extended to the entire length of the body of chosen shape.

It was established that the solution is instable for values of l_c close (on the right) to l_i: the perturbation in this case was the discreteness of the calculations although they were performed with very high accuracy. As an example, we consider the results of calculations taking into account deceleration (Fig. 3). It is evident that the curves of $\omega(\xi)$ obtained by the trapezoid method differ considerably for different numbers of partition points N_l on the integration segment $0 \leqslant l \leqslant 1$. The number of partition points on unit length of the path during integration using the Runge–Kutta method was fixed: $n_\xi = 15$. Curve 1 in Fig. 3 corresponds to the value $N_l = 400$. As N_l increases, the curves are shifted from it in different directions, which indicates a manifestation of computational instability rather than insufficient accuracy of the calculations. It should be noted that a small change in the parameters ($l_c = 0.59$ or $\tau = 1.3$) leads to stabilization: all three curves coincide.

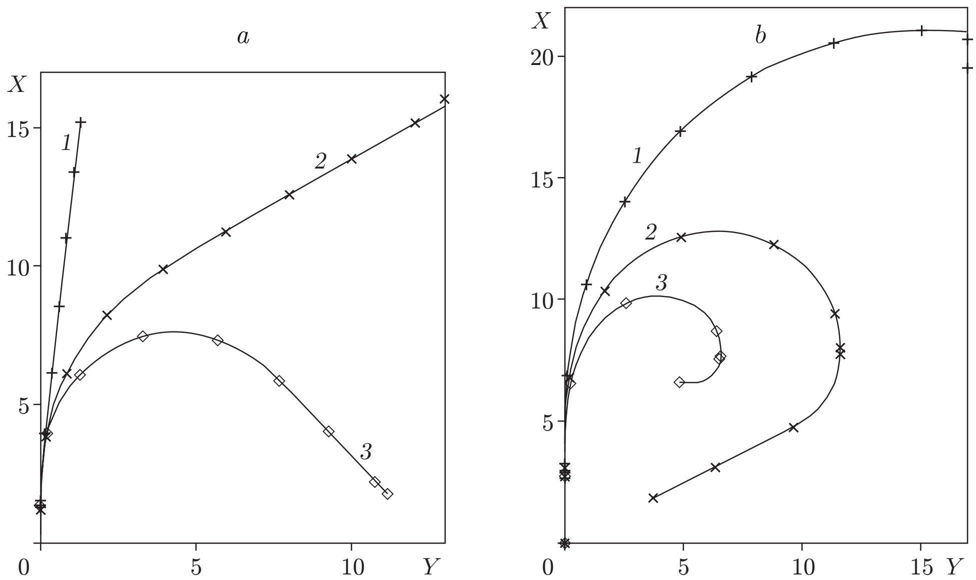

Fig. 4. Paths of light (a) and massive (b) impactors for $R_0 = 0.4$, $\beta_0 = 2$, $\beta_* = 0$, $æ_0 = 1$, $\omega_0 = -\eta_0 = 0.4$, and $\tau = 0.5$: (a) $D_0 = 0.3$ and $l_c = 0.58$ (1), 0.62 (2), and 0.66 (3); (b) $D_0 = 0.06$ and $l_c = 0.55$ (1), 0.59 (2), and 0.63 (3).

5. Effect of Determining Parameters on the Path of Motion with Deceleration. During solution of the problem (5) and (6) for $æ \neq$ const, we found the coordinates of the center of mass of the body X and Y beginning with the entry into the half-space $X > 0$ and the path $X = X(Y)$. An analysis of the results shows that the plastic friction τ has a significant effect on the path length and, as noted above, facilitates inhibition of instability. With a change in the position of the center of mass l_c (considered in the present section as a free parameter independent of body shape and other parameters), the motion path changes qualitatively (and several times). For very high velocities, the path length and curvature are in direct proportion to the quantity D, which is determined mainly by the density ratio. Figure 4a shows curves whose shape is close to some paths of more massive ($D_0 = 0.115$) pointed impactors [14]. The straight-line path (curve 1) corresponds to stable motion and the other two paths (curves 2 and 3) have an initial segment shaped like an arc of a circle, followed by a segment of straight-line motion, in agreement with the theoretical conclusion that the stability margin increases as the velocity decreases. If the velocity increases by a factor of two, the straight-line segment disappears, the paths take a shape close to an arc of a circle, in agreement with the results of analysis for "frozen" axial velocity.

If the separation is preserved near the rear points of a body of a different shape with a nonzero separation angle [$\beta_0 = 1.5$ and $\beta_* = b(1) = 0.3$] and $R_0 = 0.4$, $D_0 = 0.06$, and $l_c = 0.52$; 0.55; 0.58, then the path shapes are close to the shape of the curves presented in Fig. 4a.

In the case of a very massive impactor ($D_0 = 0.06$) made from, e.g., a tungsten alloy and penetrating into volcanic rock of low density (pumice), path elongation in stable motion is accompanied by new nonlinear effects: weakly curved motion is ended by a sharp rotation of the body because of large angles of attack (Fig. 4b). This is due to the occurrence of a secondary maximum of the angular velocity of rotation ω on the curve of $\omega(\xi)$. This effect was not observed in the case of pointed bodies [14] and can be explained by a considerable broadening of the bifurcation zone $l_s - l_a$ for blunt bodies and a change in the nature of the dependence of the path parameters γ_* and Δ_* on the axial velocity.

For $R_0 = 0.2$ and $D_0 = 0.115$ (Fig. 5), the elongation path effect due to a decrease in the head resistance is more significant than the deceleration effect due to plastic friction. A factor of two increase in the initial velocity ($æ_0 = 0.25$) (Fig. 6a) and an increase in values of l_c (Fig. 6b) lead to an increase in the path curvature due to growth in the instability margin $l_c - l_i$ (the higher the penetration velocity, the smaller the value of l_i, as a rule). An increase in the margin only due to a change in l_c (the Fig. 6b), unlike in the case of increasing entry velocity, leads to a sharp decrease in the path length because of rapid growth of perturbations.

The shape of the curves in Fig. 4a does not change if the separation angle is not equal to zero ($\beta_* = 0.5$) and the center of mass is slightly shifted to the body nose ($l_c = 0.55$, 0.6, and 0.65). In this case, $l = 7/12$,

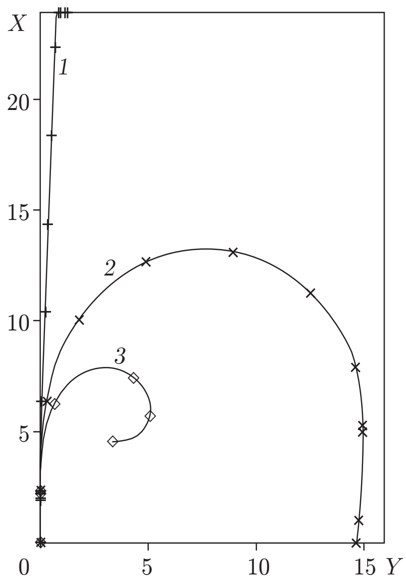

Fig. 5. Paths of a body of moderate density ($D_0 = 0.115$) for $R_0 = 0.2$, $\beta_0 = 2$, $\beta_* = 0$, $æ_0 = 1$, $\omega_0 = -\eta_0 = 0.4$, and $\tau = 1$: $l_c = 0.52$ (1), 0.6 (2), and 0.68 (3).

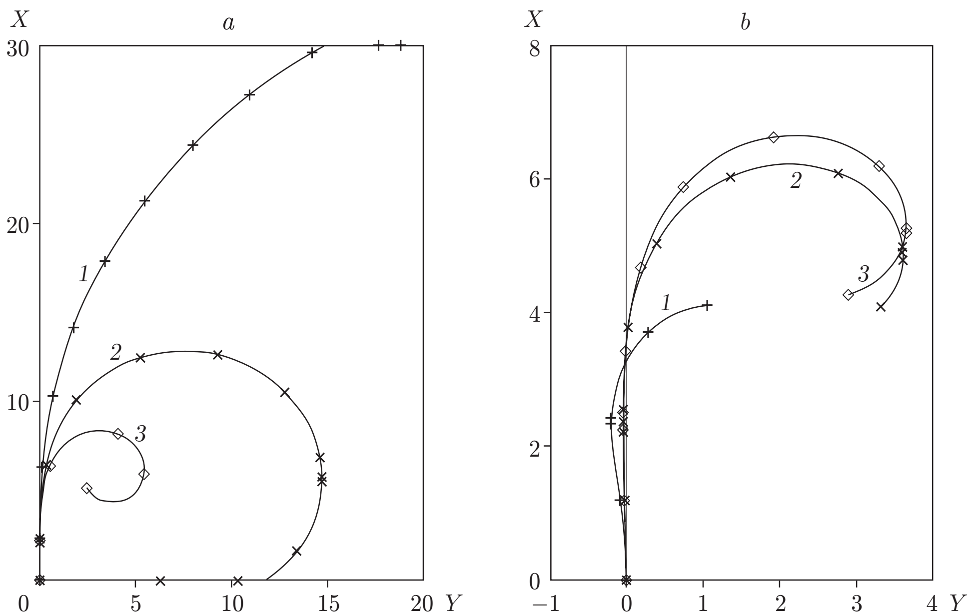

Fig. 6. Change in the impactor paths with increase in the initial velocity (a) and instability margin (b): (a) $l_c = 0.52$ (1), 0.6 (2), and 0.68 (3); (b) $l_c = 0.69$ (1), 0.71 (2), and 0.73 (3).

which corresponds to the position of the separation point for symmetric flow. When the separation angle varies from $\beta_* = 0$ (Fig. 5) to $\beta_* = 0.8$, the paths are almost identical to the curves in Fig. 6a, as in the case of a factor of two increase in the entry velocity. This indicates that variation of the separation parameter (and, hence the choice of a separation model) has little effect on the main qualitative regularities of motion and the classification of paths remains unchanged.

6. Blunt Cone. A cone ($\beta_0 = 1$ and $\beta_* = 0$) and a cylinder and their combinations with curved-meridian elements are degenerate body shapes in relation to separation: according to the proposed model, finite separation spots appear instantaneously. In the neighborhood $-l_c < \pm\omega^{-1}(1 \pm \eta) < 1 - l_c$, the cone first moves in a continuous flow regime and its subsequent motion is determined by the critical position of the center of mass l_g [13].

The calculated paths of a cone for $R_0 = 0.4$, $\beta_0 = 1$; $b_* = 0$, $D_0 = 0.3$ and 0.06, $æ_0 = 1$, -0.4, and 0.4; and the values of $l_c = 0.58$, 0.61, 0.64, 0.70, 0.74, and 0.78 correspond qualitatively to those given in Fig. 4b and Fig. 6b. The difference lies in the fact that in this case, the values of the angle of attack and rotation velocity before complete stop are larger. In addition, there are no straight-line path segments in the region of instability: the path curvature increases and the paths become shorter than those in the case of a parabolic body shape.

We note that for a cone of uniform density, $l_g = 0.6345$ and if it is large enough, its motion is unstable. Cones are frequently used in penetration experiments; therefore, in comparing the penetrations of axisymmetric and three-dimensional configurations, it is necessary that the stability criteria be equivalent.

7. Calculation of Force Characteristics of Dynamic Bending. We consider the problem of the bending of a thin elastic rod of nonuniform length with traction-free ends under lateral quasistatic loading due to interaction with a medium during high-velocity penetration. The principal vector and the principal moment of these loads are not equal to zero; therefore, we decompose the motion of the elastic body into components: rid body motion and dynamic bending. Accordingly, the dimensionless external lateral load q_0 is represented as a superposition of an equivalent non-self-balanced load that does not cause bending and a self-balanced residue $q(l, \xi)$:

$$q_0(l,\xi) = m(l)[P_0/m_0 + P_1(l - l_c)/J] + q(l,\xi) \equiv æ\Phi(l,\xi)R(l),$$

$$P_j(\xi) = \int_0^1 q_0(l,\xi)(l - l_c)^j\,dl, \qquad m_0 = \int_0^1 m(l)\,dl.$$

Here $m(l) = \pi\rho(l)r^2(l)$ is the mass per unit length and P_j is the resultant of the forces. The shear force Q and the bending moment M are determined by solving the boundary-value problem

$$\frac{dQ}{dl} = q(l,\xi), \qquad \frac{d^2M}{dl^2} = q(l,\xi), \qquad Q = 0, \qquad M = 0, \qquad l = 0, 1$$

with the normalization

$$q = \frac{q_y}{B}, \qquad Q = \frac{Q_y}{BL}, \qquad M = \frac{M_y}{BL^2}, \qquad B = b_f\tau_d r_{\max}$$

(the subscript y denotes dimensional quantities). The maximum tensile stress $\sigma_{x,\max}$, its dimensionless analog $\sigma_{\max}$ in a certain cross-section of the rod, and the strength margin n are defined by the well-known formulas

$$\sigma_{\max} = \frac{M}{R^3} = \frac{\pi\varepsilon^2\sigma_{x,\max}}{4b_f\tau_d}, \qquad n = \frac{\Sigma_*}{\Sigma}, \qquad \Sigma = \max\{\sigma_{\max}(l)\}, \qquad 0 < l < 1, \tag{9}$$

where Σ_* is the dimensionless tensile strength, which is related to its dimensional analog σ_* by a formula similar to the expression for $\sigma_{\max}$ in (9).

To ensure a specified position of the center of mass by selecting the mass per unit length $m(l)$, we assume that the impactor consists of two materials with density $\rho = \rho'$ for $0 < l < l_1$ and $\rho = \rho''$ for $l_1 < l < 1$; $\gamma = \rho'/\rho''$. Then,

$$l_c = \frac{I_1}{I_0}, \qquad I_k = \int_0^1 l^k m(l)\,dl, \qquad J = \int_0^1 (l - l_c)^2 m(l)\,dl. \tag{10}$$

The ratio γ and the moment of inertia J are found by choosing a value of l_1 for a certain specified value of l_c from Eq. (10), and then the parameter j_0 is calculated by one of formulas (4).

In the case of a parabolic body shape (7), the calculation formulas become

$$\gamma = \frac{l_c[F_1(1) - F_1(l_1)] + F_2(l_1) - F_2(1)}{F_2(l_1) - l_cF_1(l_1)},$$

$$j_0 = \frac{(\gamma - 1)F_1(l_1) + F_1(1)}{(\gamma - 1)[l_c^2F_1(l_1) - 2l_cF_2(l_1) + F_3(l_1)] + l_c^2F_1(1) - 2l_cF_2(1) + F_3(1)},$$

$$F_k = l^k\Big(\frac{R_0^2}{k} + \frac{2R_0R_1l}{k+1} + \frac{(R_1^2 - 2R_0R_2)l^2}{k+2} - \frac{2R_1R_2l^3}{k+3} + \frac{R_2^2l^4}{k+4}\Big),$$

$$R_1 = \beta_0(1 - R_0), \qquad R_2 = (\beta_0 - 1)(1 - R_0), \qquad k = 1, 2, 3.$$

TABLE 1

R_0	l_0	l_c	γ	j	n	$l_{\max}$	$S_{\max}$	$\Delta_{\max}$
		0.61	2.361	21.37	0.92	0.001	3.0	0.455
0	0.65	0.62	2.108	21.16	0.30	0.038	20.0	1.0
		0.63	1.887	21.04	0.26	0.001	20.0	1.0
		0.59	2.317	18.57	1.30	0.201	2.6	0.468
0.1	0.60	0.61	1.889	18.47	0.40	0.190	20.0	1.0
		0.63	1.541	18.65	0.33	0.190	20.0	1.0
		0.58	2.053	17.11	1.69	0.276	2.93	0.502
0.2	0.60	0.60	1.686	17.05	0.51	0.274	20.0	1.0
		0.62	1.386	17.23	0.45	0.273	20.0	1.0
		0.57	1.819	15.45	2.44	0.334	4.4	0.413
0.3	0.55	0.59	1.512	15.79	0.78	0.300	20.0	1.0
		0.61	1.253	14.52	0.84	0.268	20.0	1.0
		0.57	1.483	14.74	3.17	0.398	5.9	0.656
0.4	0.55	0.59	1.238	15.14	1.12	0.338	20.0	1.0
		0.61	1.030	15.31	1.10	0.355	20.0	1.0

Note. $\beta_0 = 2$, $\beta_* = 0$, $\omega_0 = 0.4$.

TABLE 2

R_0	l_0	l_c	γ	j	n	$l_{\max}$	$S_{\max}$	$\Delta_{\max}$
		0.65	1.515	21.06	3.58	0.044	2.53	0.130
0	0.65	0.66	1.358	21.21	3.50	0.001	3.13	0.141
		0.67	1.217	21.45	0.21	0.001	20.0	1.0
		0.66	1.124	19.80	3.88	0.310	3.8	0.162
0.1	0.70	0.67	1.009	19.95	0.31	0.190	20.0	1.0
		0.68	0.906	20.18	0.34	0.178	20.0	1.0
		0.66	0.926	18.26	4.54	0.415	3.27	0.175
0.2	0.65	0.67	0.835	18.60	0.58	0.243	20.0	1.0
		0.68	0.751	19.03	0.74	0.218	20.0	1.0
		0.66	0.766	16.84	5.34	0.480	2.67	0.185
0.3	0.70	0.67	0.693	17.09	5.43	0.478	4.07	0.2
		0.68	0.627	17.40	0.96	0.495	20.0	1.0
		0.68	0.526	16.39	6.52	0.538	3.73	0.214
0.4	0.70	0.69	0.477	16.80	0.25	0.465	20.0	1.0
		0.70	0.431	17.28	0.19	0.463	20.0	1.0
		0.70	0.366	16.49	7.90	0.628	6.4	0.2
0.5	0.70	0.71	0.331	17.08	0.106	0.473	20.0	1.0
		0.72	0.297	17.77	0.087	0.475	20.0	1.0

Note. The calculations were performed for $\beta_0 = 2$, $\beta_* = 0$, and $\omega_0 = 0.1$.

An analysis shows that the dependence $\sigma_{\max}(l)$ is continuous at the point $l = 0$ (i.e., remains finite in the case of a pointed body, too) but it has an absolute maximum at this point; nevertheless, fracture begins from the body nose. Thus, the body nose should be blunted to ensure higher strength.

The influence of the bluntness radius R_0 on the magnitude of the safety margin, the position of the point of fracture onset and the time of attainment of the dangerous condition is studied for a body of parabolic shape (7) by varying the position of the center of mass and the bluntness radius for the following parameter values (the axial velocity is frozen): $\beta_0 = 2$, $\tau = 1$, $D_0 = 0.115$, $\beta_* = 0$, $b_f = 7$, $\tau_d = 5$ MPa, $\sigma_* = 1$ GPa, and $æ = 2$.

The presence of a disk-shaped bluntness does not imply flow separation immediately behind the disk: separation occurs when a certain limiting velocity is attained. This is prevented by two factors: the formation of a stagnation zone ahead of the disk, which "is washed off" and becomes narrower as the velocity of motion increases, and the presence of a nonzero (maximum) slope of the lateral surface of the body immediately behind the disk.

Tables 1 and 2 give the safety margin n, the distance from the body nose $l_{\max}$, and the length of the path $\xi_{\max}$ for which the maximum $\sigma_{\max}(l)$ is reached, and the length of the separation zone $\Delta_{\max}$ at the moment

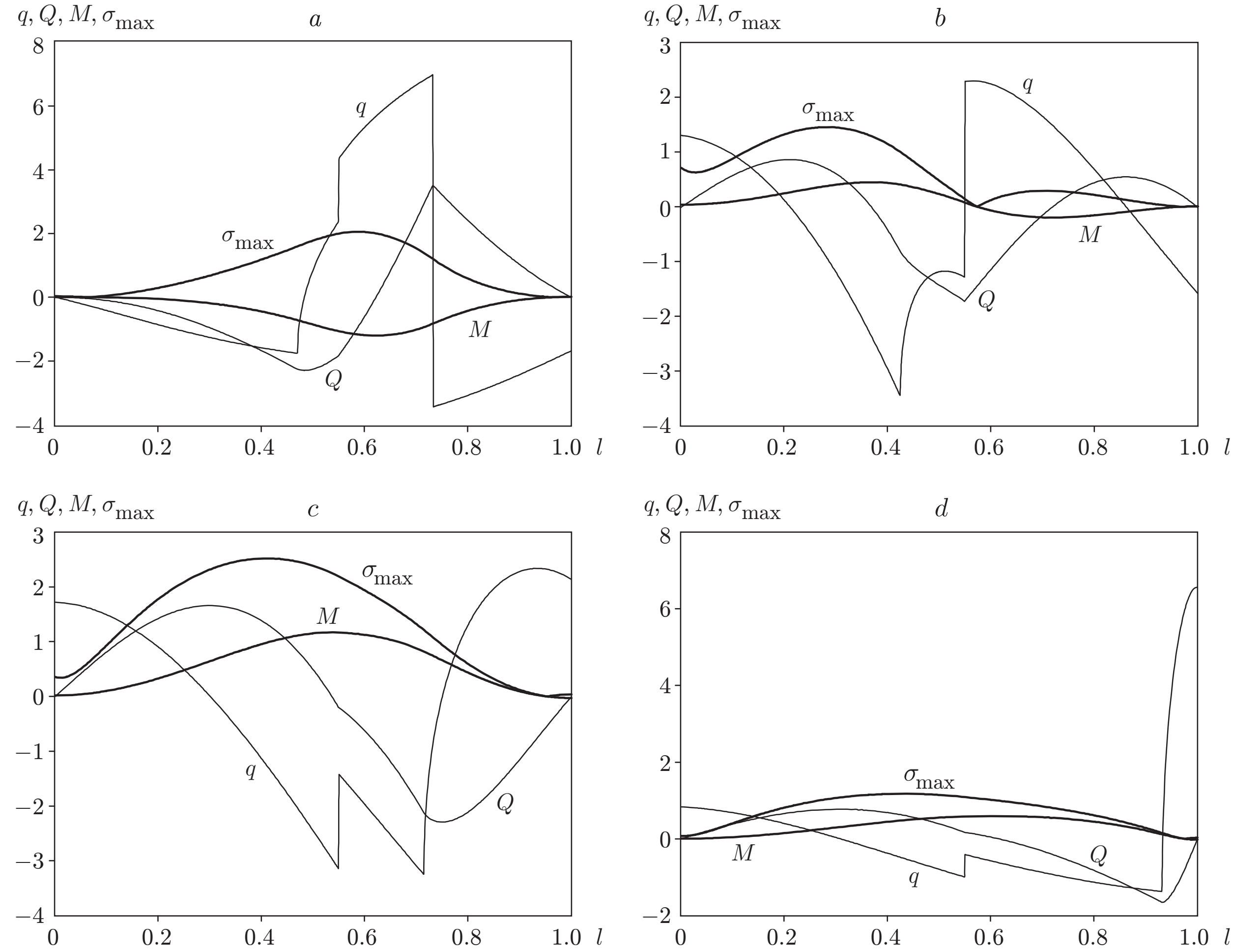

Fig. 7. Lateral loading q, shear force Q, bending moment M, and maximum cross-sectional stress $\sigma_{\max}$ versus immersion depth l for $\xi = 0.733$ (a), 1 (b), 6 (c), and 7 (d); $r_0 = 0.4$, $l_c = 0.57$, $\omega_0 = 0.4$, and $æ = 2$:

of attainment of the maximum. For each value of the bluntness radius R_0, calculations were performed for three values of the distance l_c, which corresponded to a "stable" (nearly straight-line) path and "slightly unstable" and "highly unstable" paths, using two values of initial perturbations: $\omega_0 = -\eta_0 = 0.1$ and $\omega_0 = -\eta_0 = 0.4$. From Tables 1 and 2, it follows that even in the case of a small bluntness ($R_0 = 0.1$), the dangerous point $l = l_{\max}$ is shifted from the nose to center of the body (this shift is maximal for "stable" paths). In this case, the safety margin can increase by a factor of 1.5. The indicated features are also observed when the bluntness radius increases to the value $R_0 = 0.9$; in this case, the point $l = l_{\max}$ is near the center of the body. The corresponding immersion depth $\xi_{\max}$ also depends substantially on the parameters l_c, R_0, and ω_0. It should be noted that the minimum safety margin is reached not at the moment of entry but when the body is completely immersed in the medium: in the case of nearly straight-line paths, for $\xi_{\max} \approx 2.5$–6.0 and in the case of curved "unstable" paths, at the moment the body enters a stationary path for which the calculated perturbation is maximal.

The safety margin n grows with increase in bluntness radius, other things being equal. For $0 \leqslant R_0 \leqslant 0.1$, the increment in n is nearly linear and changes considerably, and then, for $R_0 \geqslant 0.1$, it does not decrease although the comparison can be only indirect because it is made for different curves of growth or damping of perturbations of ω and η.

An analysis of data on the dimension of the separation zone $\Delta_{\max}$ shows that dangerous stresses occur, as a rule, for the maximum dimension of the zone, which indirectly correlates with the maxima of ω and η.

Figure 7 shows distributions of the lateral bending load q, the shear force Q, the bending moment M, and the maximum cross-sectional tensile stress $\sigma_{\max}$ for various values of ξ. The jump for $l = l_1 = 0.57$ is due to a jump of inertial forces (responsible for rigid body motion) subtracted from the complete lateral loading, because of a density jump in this cross section. This is followed by a sudden (typical of a boundary layer) change in this load at the beginning of the separation zone.

Conclusions. From the results of the present study of the stability of straight-line motion of a thin blunt body, it follows that large perturbations reduce the stability margin in the small to a greater extent in this case than in the case of pointed bodies. The studies showed the possibility of occurrence of curved paths that are qualitatively close to specified ones with considerably different separation parameters: straight-line, curved on the initial segment and then straight-line (in this case, the body can move away, move parallel to or approach the target surface, so that it can return to this surface or stop inside the target), curved, and close to an arc of a circle. Thus, the main characteristics of the examined motion depend weakly on the choice of a separation criterion, which needs to be refined. The distribution of the dynamic loads acting on a thin body from the medium is similar to the distribution in the boundary layer.

This work was supported by the Russian Foundation for Basic Research (Grant No. 02-01-00259).

REFERENCES

1. S. S. Grigoryan, "Approximate solution of the problem of body penetration into soil," *Izv. Ross. Akad. Nauk. Mekh. Zhidk. Gaza*, No. 4, 18–24 (1993).
2. Yu. K. Bivin and I. V. Simonov, "Estimated depths of penetration of rigid bodies into soils at hypersonic entry velocities," *Dokl. Ross. Akad. Nauk.*, **328**, No. 4, 447–450 (1993).
3. I. V. Simonov, "Cavitational penetration of bodies of minimum resistance into a high-strength medium," *Prikl. Mat. Mekh.*, **57**, No. 6, 111–119 (1993).
4. V. M. Fomin, A. I. Gulidov, G. A. Sapozhnikov, et al., *High-Velocity Interaction of Bodies* [in Russian], Izd. Sib. Otdel. Ross. Akad. Nauk, Novosibirsk (1999).
5. A. V. Bogdanov, A. V. Nikolaev, G. A. Skuridin, et al., "One method of studying the Earth's group planets," *Kosmich. Issled.*, **24**, No. 4, 591–603 (1988).
6. A. V. Zaitsev, A. V. Dobrov, V. A. Kotin, and I. V. Simonov, Possibilities of the hypervelocity impact experiment in frames of demonstration project "Space patrol," Int. *J. Impact Eng.*, **20**, 849–860 (1997).
7. I. V. Simonov, S. A. Fedotov, and O. B. Khavroshkin, "Near-catastrophe state of geophysical objects, triggering, and penetration," *Dokl. Ross. Akad. Nauk*, **347**, No. 6, 811–813 (1996).
8. A. Ya. Sagomonyan, *Penetration* [in Russian], Izd. Moscow Univ., Moscow (1974).
9. L. M. Flitman, "Subsonic axisymmetric elastoplastic flow of pointed thin bodies of revolution," *Izv. Akad Nauk SSSR, Mekh. Tverd. Tela*, No. 4, 155–164 (1991).
10. L. M. Flitman, "High-velocity elastoplastic flow without separation over a blunt body," *Prikl. Mat. Mekh.*, **54**, No. 4, 642–651 (1990).
11. Yu. K. Bivin, V. V. Viktorov, and B. Ya. Kovalenko, "Determining the dynamic characteristics of soils by a penetration method," *Izv. Akad. Nauk SSSR, Mekh. Tverd. Tela*, No. 3, 105–110 (1980).
12. Yu. K. Bivin, V. A. Kolesnikov, and L. M. Flitman, "Determining the mechanical properties of a medium using a dynamic penetration method," *Izv. Akad Nauk SSSR, Mekh. Tverd. Tela*, No. 5, 181–185 (1982).
13. I. V. Simonov, "Dynamic stability of an oblong body of revolution in an elastoplastic medium with flow separation," *Prikl. Mat. Mekh.*, **64**, No. 2, 311–320 (2000).
14. I. V. Simonov, "Classification of the paths of plane–parallel motion of a body of revolution in a high-strength medium with flow separation," *Dokl. Ross. Akad. Nauk*, **386**, No. 2, 198–202 (2002).
15. K. Yu. Osipenko and I. V. Simonov, "Model for the spatial dynamics of a body of revolution during interaction with a low-strength medium and asymmetric cavitation," *Izv. Ross. Akad. Nauk, Mekh. Tverd. Tela*, No. 1, 151–161 (2002).
16. K. Yu. Osipenko and I. V. Simonov "Supersonic flow of a porous medium over a cone," *Izv. Ross. Akad. Nauk, Mekh. Tverd. Tela*, No 2, 87–95 (2001).